

Electronic Supplementary Information for: Role of aluminium hydrides in localised corrosion of aluminium revealed by operando Raman spectroscopy

Erlind Mysliu¹

Otto Lunder²

Andreas Erbe^{1*}

¹ Department of Materials Science and Engineering, NTNU, Norwegian University of Science and Technology, 7491 Trondheim, Norway

² SINTEF Industry, 7465 Trondheim, Norway

* Corresponding author, FFC-Raman@the-passivists.org (Andreas Erbe)

Contents

1	Additional experimental information	2
2	Surface morphology	3
3	Assignment of features in experimental Raman spectra	4
4	Video of filiform corrosion	11

1 Additional experimental information

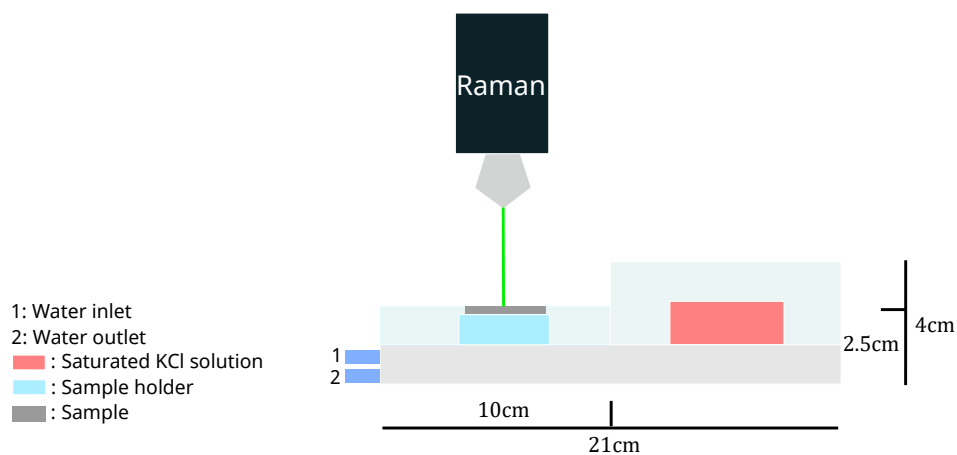


Figure S1: Home-made cell for In-situ Raman analysis. Schematic representation (top), set-up used during in-situ measurements and top view of the cell used for in-situ measurements (bottom). In the bottom right picture it is also shown the temperature and humidity sensor. Approximate dimensions are schematically indicated in the top image. The width of the cell (not shown in the top image) is 10 cm.

The raw data associated with this study is available via the BIRD repository of Norwegian Higher Education Institutions.[1]

2 Surface morphology

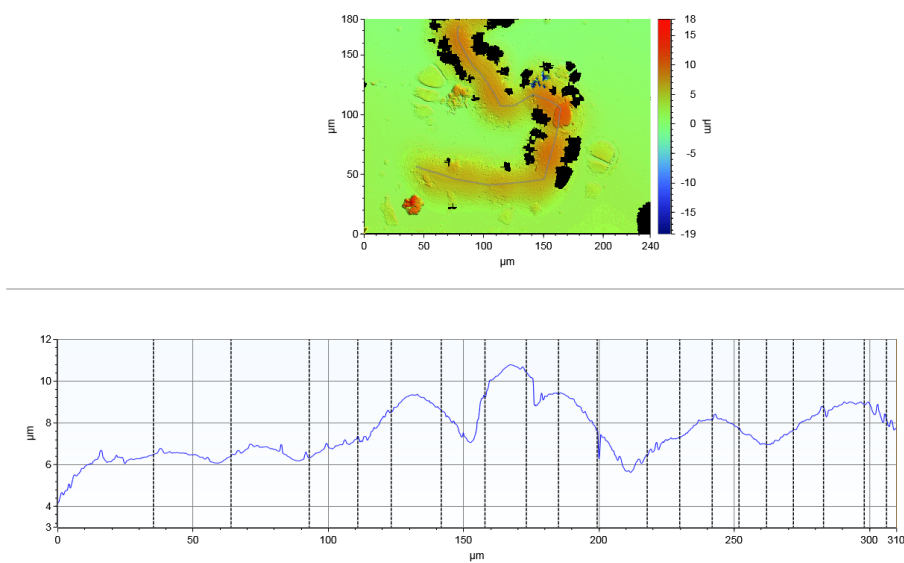


Figure S2: Filament tail with alternating regions of higher and lower lifting of coating. Height profile at the bottom follows the line along the filament shown in the top image.

3 Assignment of features in experimental Raman spectra

This section contains a detailed reasoning for the assignment of the vibrational spectra. The reasoning is summarised in Main-Section 3.2. The corresponding spectra are shown in Main-Fig. 5 and 6, supplemented by Fig. S3-S7.

Despite the high confocality of the setup, combined with a computational procedure to separate components, it is possible that components from the coating contribute to the spectra at the coating/metal interface. Such components can (i) be components from the intact coating, or (ii) components from degradation products of the coatings. The components (i) from the intact coating are, however, well known (Fig. S3), and major peaks characteristic for the intact coating are missing at the interface. A comprehensive peak assignment for the intact coating is shown in Tab. S2. As to (ii) components from coating degradation products, one needs to look into possible degradation products.

From the knowledge about the degradation of polyacrylate model coatings [2, 3], and from general chemical considerations, the interfacial region does not contain contributions from organic degradation products of the coatings. The absence of CH stretching modes in the spectral region $2800\text{-}3000\text{ cm}^{-1}$, which also feature strongly in the spectrum of the pure coating, is the strongest argument for the absence of organic components. Acrylates can suffer hydrolysis, and though there are arguments for [4] and against [2] hydrolysis as contributing factor of interfacial failure, the products are carboxylates or carboxylic acid. No traces of typical carboxylate modes can be identified in the spectra, though some of the peaks in the region $1000\text{-}1750\text{ cm}^{-1}$ are at positions where they potentially could originate from carboxylates. Overall, we assign the remaining spectral features in Main-Fig. 5c thus to the presence of inorganic aluminium corrosion products, which must be reaction products between aluminium, N_2 , H_2O , $\text{HCl}_{(\text{aq})}$, O_2 , and CO_2 . Under the conditions of this work, the main corrosion products are supposed to be aluminium [(oxy)hydr]oxides, aluminium hydroxycarbonates and aluminium chlorides.

In these in situ experiments with active filaments, the presence of water would be expected, and the broad peak from $3000\text{-}3600\text{ cm}^{-1}$ is typical for the water OH stretching modes [5, 6]. In addition, hydroxide corrosion products must contribute to this peak, evidenced by the sharp component at 3075 cm^{-1} which is in a region where typically modes of structural OH are observed in minerals [6]. The broad band may also contain more contributions of different amorphous (oxo)hydroxides [7]. However, the discrimination between the different components is made difficult by the overlapping peaks and the presence of amorphous phases that causes peak broadening [5, 8, 9]; a further detailed assignment shall not be attempted in this work. If stretching modes are observed, corresponding OH bending modes must also be present. The peak at 1607 cm^{-1} , with a shoulder at higher wavenumbers, can easily be attributed to the OH_2 bending mode of adsorbed or included water. A more detailed discussion of Al-OH bending modes will be given below; there is, however, obvious evidence for the presence of hydroxides in the head.

The four principal hydroxides/oxyhydroxides of aluminium are gibbsite $\gamma\text{-Al}(\text{OH})_3$, bayerite $\alpha\text{-Al}(\text{OH})_3$, boehmite $\gamma\text{-AlOOH}$ and diasporite $\alpha\text{-AlOOH}$. A comprehensive analysis of the Raman spectrum and structure of these species has been published in different works [9–14]. In addition, oxides with different level of disorder may form; the disorder complicates a thorough assignment of the spectra as it changes selection rules common for the crystalline phases. In line with other literature [15, 16], we will therefore use both IR and Raman literature for the assignment. Peaks at around 520 cm^{-1} , 600 cm^{-1} and 840 cm^{-1} are commonly found in aluminium oxidation products and related compounds

[7, 9, 15–24]. The observed broad peak around 600 cm^{-1} is representative of AlO_6 octahedra (E_g) [7, 9, 17, 22]; its presence has been related to the presence of a mixture of aluminium (oxy)hydroxides [7, 9, 22], though they are also observed in a number of systems where the presence of hydroxides is not immediately obvious [15, 21, 25]. Similar compounds can be observed on the surface of aluminium after alkaline dissolution. This peak has been observed analysing the surface of an aluminium sample exposed to a concentrated NaOH solution for 5 minutes where the formation of aluminium oxides and aluminium (oxy)hydroxide compounds is supposed to take place. The spectrum is shown in Fig. S4. The band at $\approx 520\text{ cm}^{-1}$ has been assigned to the Al^{3+} -oxygen symmetric stretching mode of the hexaquo coordinated aluminium $[\text{Al}(\text{OH}_2)_6]^{3+}$ in aqueous solutions in presence of AlCl_3 [26, 27]. The band around 840 cm^{-1} has previously been assigned to $\text{Al}-\text{O}$ vibration of AlO_4 tetrahedrons in different aluminium oxides, hydroxides and oxyhydroxides [15, 18, 20]. Summarising, there is evidence for the presence of aluminium oxides or oxyhydroxides in the system, both with tetrahedrally and octahedrally coordinated aluminium ions. It is worth investigating the literature spectra of related compounds for further peaks which are present in our spectra and can help assign remaining peaks; the experimental spectra show in addition peaks at 1045 , 1164 , 1420 , and 1495 cm^{-1} in the head (Main-Fig. 5) and 1100 cm^{-1} in the tail (Main-Fig. 6) which are not accounted for so far.

A peak at $\approx 1160\text{ cm}^{-1}$ has been observed before for aluminium corrosion products. It is unassigned in some works [19]. In IR spectra, a peak at this position has been assigned to a surface phonon [21]. Pure γ - AlOOH shows a OH deformation mode in this region [17]. More recent computational work of H_2O on hydroxylated aluminium oxide surfaces assigns a peak in the region as 1195 - 1136 to a coupling of H_2O libration, $\text{Al}-\text{OH}$ bending and the surface phonon [28]. The coupling in the latter assignment may explain the diverging assignments in other sources. A very recent computational study shows the complexity of surface transformations and corresponding vibrational spectra of hydroxylated aluminium oxide surfaces [29].

Different works have assigned peaks in the region 1300 - 1600 cm^{-1} to bending modes of differently coordinated H_2O . For example, Raman peaks at 1388 cm^{-1} [19], and 1348 - 1356 cm^{-1} [16] have been assigned to the $\delta(\text{OH}_2)$ mode of H_2O bound to tetrahedrally coordinated Al , whereas Raman peaks at 1410 cm^{-1} [16], or 1452 cm^{-1} and 1600 cm^{-1} [19], have been assigned to $\delta(\text{OH}_2)$ modes of H_2O coordinated to octahedrally coordinated Al [19]; it is not clear from the discussion in [19] why the latter yields two peaks. In a temperature-dependent IR reflection study, peaks at 1380 cm^{-1} have been assigned to “water molecules coordinated on tetrahedral ... aluminium” and peaks at 1580 cm^{-1} to “water coordinated on ... octahedral aluminium”; water at bridge sites was assigned to a bending mode at 1460 cm^{-1} [30]. On the other hand, ab initio molecular dynamics calculations of water adsorbed on α - Al_2O_3 surfaces yielded peaks at 1600 - 1663 cm^{-1} of the water $\delta(\text{OH}_2)$ [28, 31], and no other OH related peaks in the region 1200 - 1700 cm^{-1} . For $\text{Al}(\text{OH})_3$, the IR spectra in some references showed small peaks slightly below [32], or above [13] 1400 cm^{-1} ; at the same time, Raman spectra were featureless in the region 1000 - 1500 cm^{-1} [33, 34]. The high pressure δ - AlOOH showed a weak peak slightly above 1300 cm^{-1} [34]. $\text{Al}-\text{O}-\text{H}$ bending modes should be at wavenumbers lower than the bending mode of H_2O , e.g. at 1380 cm^{-1} for H_2O_2 [35]. Therefore, we assign the peak at 1420 cm^{-1} for consistency reasons to the bending mode of $\text{Al}-\text{O}-\text{H}$, which is not assigned in many of the previous works [16, 19, 30]. This assignment is in line with an IR assignment for a broad peak centred at 1350 cm^{-1} from our group for aluminium after alkaline etching [36]. The mode corresponding to the peak at 1420 cm^{-1} must be from different species than the species causing the mode at 1160 cm^{-1} , which strongly couples to $\text{Al}-\text{O}$ stretching

modes [29].

While some works on well characterised aluminium oxyhydroxides show a peak in the region around 1050 cm^{-1} [9, 11, 12, 37] which is in the vicinity of the peak observed here at 1045 cm^{-1} , all these literature spectra have completely different features in the region $200\text{-}700\text{ cm}^{-1}$. Reference spectra of gibbsite, bayrite, diaspore and boehmite show many characteristic peaks between $200\text{-}700\text{ cm}^{-1}$, very different from the spectra observed here [9, 12]. Our OH stretching mode region shows none of the gibbsite characteristic peaks [14, 34], which may however be caused by the overlapping water peak. Thus, we see little evidence for the presence of the traditional aluminium oxyhydroxides in the head region based on their spectra reported in the literature.

Carbonates show prominent, characteristic Raman peaks [38]. The carbonate ion itself has a Raman-active symmetric stretching mode at $\approx 1070\text{ cm}^{-1}$, and an IR-active symmetric stretching mode at $\approx 1390\text{ cm}^{-1}$, e.g., in CaCO_3 . In HCO_3^- , because of the break of symmetry, the spectrum becomes more involved [38]. Because of the acid-base properties of Al_2O_3 and CO_2 , a simple aluminium carbonate does not exist, however, aluminium and carbonate-containing species stabilised by other cations or anions are well known. For carbonate-rich aluminium hydroxide gel the main broad Raman peak ranging from 1060 cm^{-1} to 1170 cm^{-1} was found to peak at 1120 cm^{-1} [39–41]. The Raman peak positions of selected important aluminium and carbonate-rich minerals extracted from the RRUFF database [42] are compiled in Tab. S1; all peaks in the region characteristic for the symmetric carbonate stretching mode are between 1060 and 1130 cm^{-1} . Based on this evidence, we assign the peak at 1100 cm^{-1} observed in the tail to the symmetric stretching mode of a carbonate. The peak at 1045 cm^{-1} is too low compared to many common carbonates to represent such a peak [38].

Chlorides are frequently incorporated into solid corrosion products from chloride-containing solutions. With the involvement of heavy atoms, the respective vibrational frequencies must be located at low wavenumbers. Raman active modes for molecular AlCl_3 and Al_2Cl_6 have been reported at 342 cm^{-1} (A_g ; shifted up to 350 cm^{-1} for the AlCl_4^- ion [43, 44]), 523 cm^{-1} (A_g), and 613 cm^{-1} (B_{2g}) in the gas phase [45]. Some of these peaks are in the same region of the modes of aluminium (oxy)hydroxides and thus cannot be clearly detected. Here, the peak observed at 347 cm^{-1} in the tail region is assigned to the presence of Al–Cl containing species. Aluminium (oxy)hydroxides also contain peaks around 350 cm^{-1} [9, 11, 37], however, the spectra in from the tail where these peaks are observed do not show the other characteristic peaks of the corresponding (oxy)hydroxide. As those peaks are typically more prominent, we consider the assignment of the peak observed here at 347 cm^{-1} to a mode containing oxide-related species as unlikely. Solid aluminium chloride on the other hand shows as strongest features the $\nu(\text{Al}-\text{Cl})$ stretching and $\delta(\text{Al}-\text{Cl}_2)$ bending at 308 and 171 cm^{-1} [46]. In water, the main peak at 308 cm^{-1} disappears and is replaced by a peak at 350 cm^{-1} representative of the Al–Cl stretching mode in the AlCl_4^- ion [46]. In alkali chloroaluminates, the A_1 mode is also reported at $340\text{-}350\text{ cm}^{-1}$ [47]. A peak corresponding to the $\nu(\text{ClAl})$ A_g mode was reported at 342 cm^{-1} [48]. In condensed phases, chloride-based compounds tend to polymerize with the halogen atom that can be in a terminal or in a bridge position [49]. The bridging frequencies are expected to be at $\approx 345\text{ cm}^{-1}$ (A_g) while the terminal frequencies are expected at $\approx 495\text{ cm}^{-1}$ (A_g) [50]. From these considerations, we assign the peak at 347 cm^{-1} to molecular AlCl_4^- . Finally, since the water content in the tail of the filament has to be low, the AlCl_4^- ions are probably embedded in an aluminium chloride-based solid compound; in an oxide containing complex ion, the peak shifted significantly from the 350 cm^{-1} region with substitution of one chloride ligand with an oxygen ligand [51]. With all these common aluminium corrosion products, there remain three unassigned

peaks in the head region at 1045 and 1495 cm^{-1} .

Aluminium nitrides are not typical corrosion products, however, their formation cannot in principle be ruled out. The main peaks from aluminium nitride are located at 611, 654, 665 cm^{-1} with a broad weak peak at 905 cm^{-1} corresponding to $E_2(\text{high})$, $A_1(\text{TO})$, $E_1(\text{TO})$ and a combination of the $E_1(\text{TO})$ and $A_1(\text{LO})$ modes, respectively [52–55]. None of these peaks fits to any observed peak, so we can safely rule out the formation of nitrides in this system.

Based on potential measurements in aqueous solutions and thermodynamic arguments, the formation of aluminium hydrides has been suggested [56–58]. The existence of aluminium hydrides has been experimentally shown *ex situ* under highly alkaline conditions [59, 60]. The Raman spectra of different aluminium hydrides have been reported in the literature [61–66]. The most intense peaks of $\alpha\text{-AlH}_3$ at 506 and 715 cm^{-1} are not present in the spectra found here [62]. However, the $\gamma\text{-AlH}_3$ polymorph showed characteristic Al-H stretching modes at 1053 and 1487 cm^{-1} , with the former sharper and more intense than the second [61, 64, 67]. The peaks at 1045 and 1495 cm^{-1} in the spectra observed in the filament head region in this work can thus be assigned to the presence of aluminium hydride resembling $\gamma\text{-AlH}_3$, as both positions, relative intensities and width agree well with literature data [61, 64]. The peak at 1045 cm^{-1} is associated with the out-of-plane motion of the hydrogen atoms H4 in the structure reported by Wang et al. [c.f. Figure 1(b) of ref. [66]].

Table S1: Raman peak positions in cm^{-1} of some aluminium carbonate containing minerals as reported in the RRUFF database (<https://rruff.info/>) [42].

Dawsonite	Hydrocalcite	Caresite	Carbonatecyanotrichite
1505	1352	1062	1121
1096	1062	549	974
733	995		615
592	543		590
392			525
265			446
193			274
			234

Table S2: Raman peak positions for the Paraloid B 48 acrylate coating.

Peak position / cm^{-1}	Origin	Ref.
370	ν_s C–COO and δ_s in plane	[68]
488	C–COO [−] o.o.p. deformation	[68]
601	$\nu(\text{C–COO})$ $\nu_s(\text{C–COO})$	[68]
817	$\nu_s(\text{C–O–C})$	[68]
970	$\alpha\text{-CH}_3$ rock	[68]
1455	δ_a C–H of $\alpha\text{-CH}_3$ and O–CH ₃	[68]
1731	$\nu(\text{C=O})$ of C–COO	[69]
2953	$\nu_s(\text{C–H})$ of O–CH ₃ and $\alpha\text{-CH}_3$	[68]

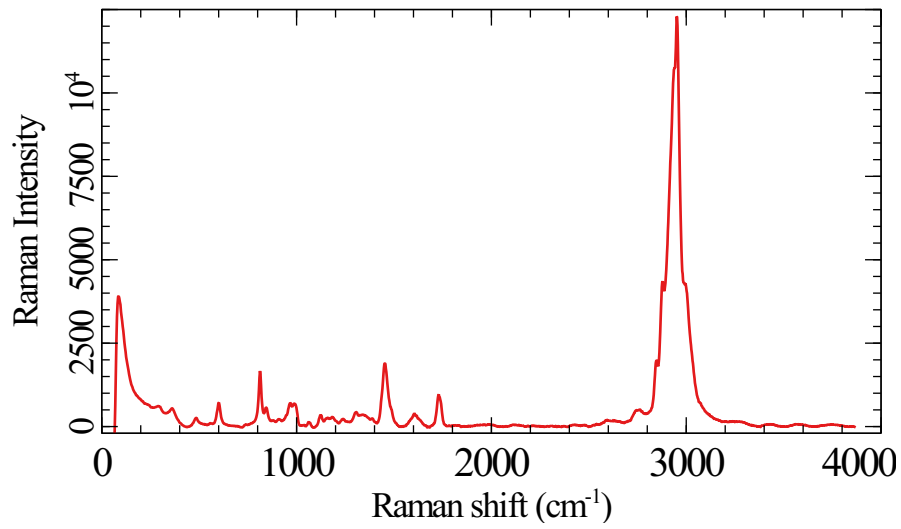


Figure S3: Spectrum of polyacrylate-based Paraloid B 48 used as model coating in this work.

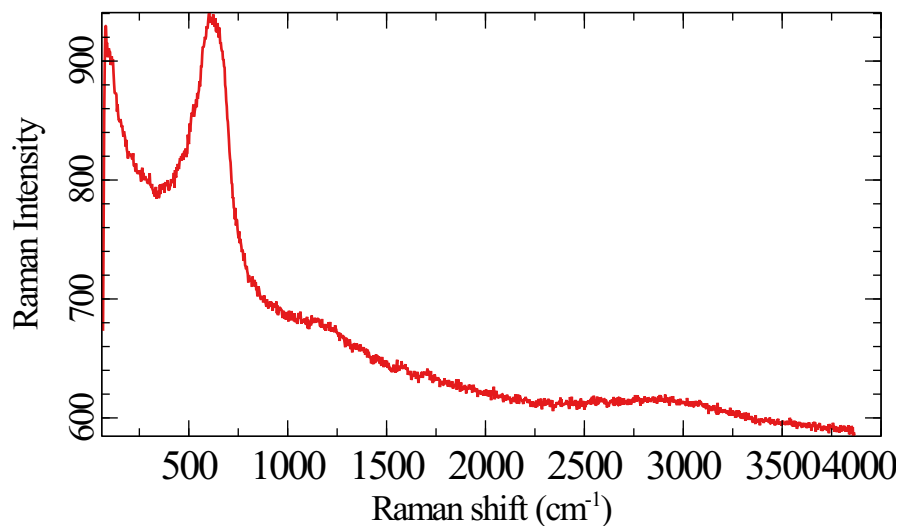


Figure S4: Spectrum of aluminium surface after alkaline etching showing the main broad peak around 600 cm⁻¹.

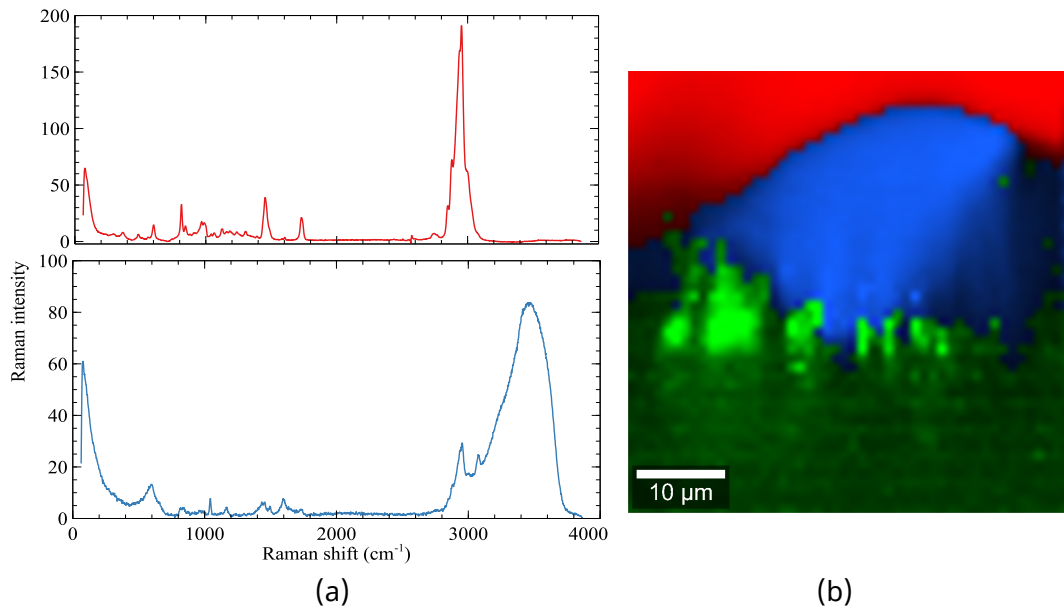


Figure S5: Depth scan in the head of the filament shown in the main article, Main-Fig. 5.

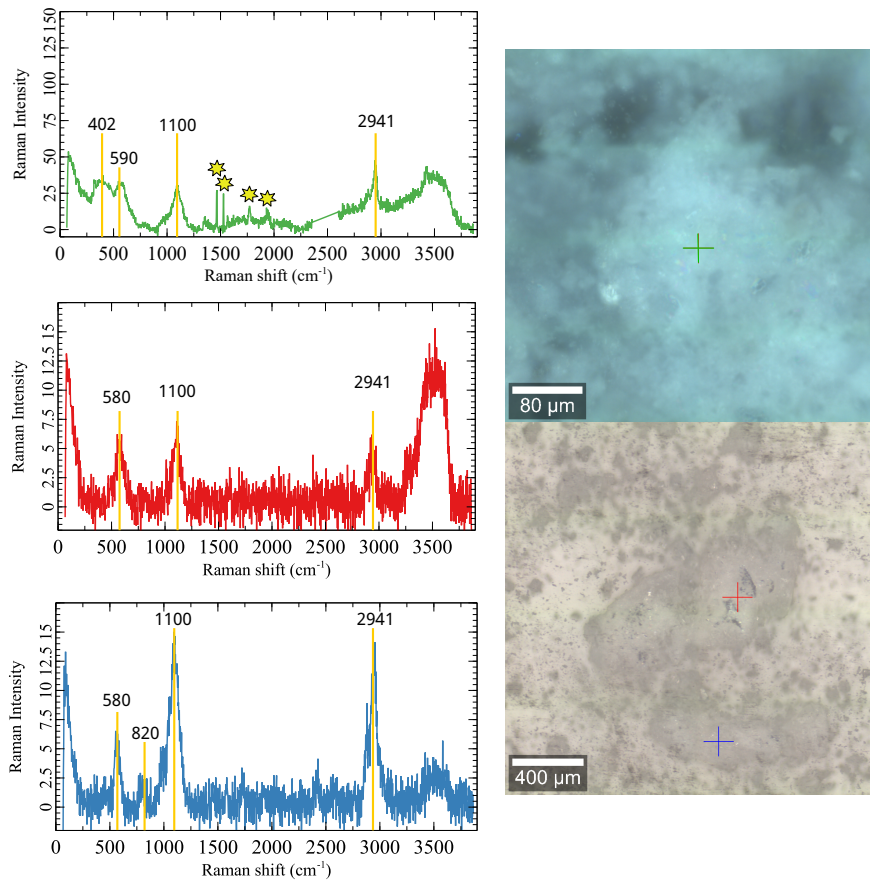


Figure S6: Corrosion products (right) and corresponding spectra (left) recorded at the cross of the respective colour. The position of the spectra is indicated by the coloured crosses. The region between 2360 cm^{-1} and 2600 cm^{-1} in the green spectrum has been removed due to the presence of a peak from the artificial light of the room. Other peaks coming from ambient light are marked with a yellow star.

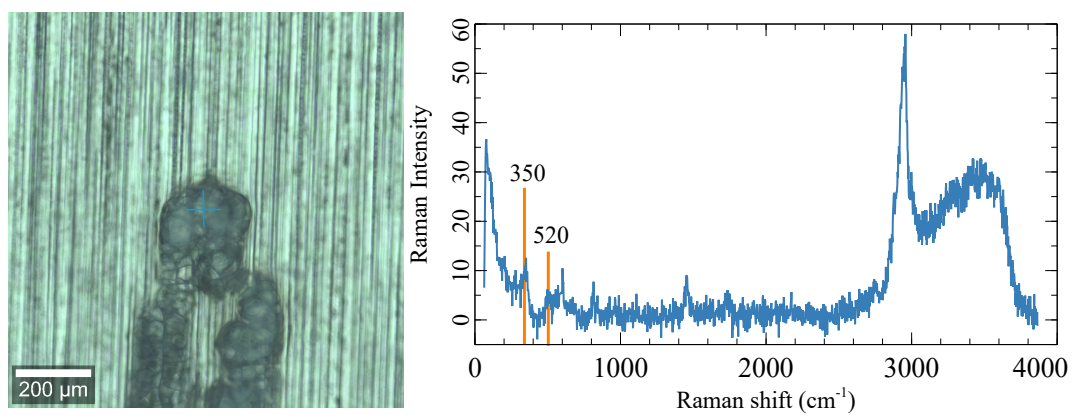


Figure S7: Micrograph of part of the tail of an inactive filament (left) and spectrum (right) showing the presence of both the peak at 350 cm^{-1} and 520 cm^{-1} . The spectrum position is indicated by the blue cross.

4 Video of filiform corrosion

The video attached (FFC_2.mp4) has been recorded using the same instrument used for the Raman measurements described in the main article. The video was created by recording an image every 100 s (0.01 frames per seconds), which was translated into 1 image per second in a raw video. The video recording took ca. 22 h. The accelerated version presented is condensed into ca. 2 min. The acceleration factor ($4\times$ or $16\times$) is shown as an inset in the video. 1 s video with acceleration $4\times$ corresponds to 400 s in real time.

The width of the filament base is $\approx 80\text{-}90\ \mu\text{m}$ both in the top part of the filament body shown during the first part of the video (low magnification, $10\times$ objective; until ca. 48 s) and at the head of the filament shown in the second part of the video (high magnification, $50\times$; from ca. 49 s). In the second part of the video, the imaged location was adjusted to accommodate for the propagation of the filament.

The artificial coating defect from where the filament started propagating is not shown. The filament was initially propagating from the top in a downward direction on the video. The initial filament became inactive but then reactivated. After a certain period of time, a the filament started propagating in the opposite direction of the initial direction along the boundary of the initial filament. The video only contains images from the second phase of propagation; the first part is difficult to capture because of the exact initiation location of the initial filament is hard to foresee.

References

- [1] E. Mysliu, O. Lunder and A. Erbe, *Data package for: Role of aluminium hydrides in localised corrosion of aluminium revealed by operando Raman spectroscopy*, BIRD, <https://hdl.handle.net/11250/3056964>, 2023.
- [2] D. Iqbal, J. Rechmann, A. Sarfraz, A. Altin, G. Genchev and A. Erbe, *ACS Appl. Mater. Interfaces*, 2014, **6**, 18112–18121.
- [3] J. S. Mondragón Ochoa, *PhD thesis*, Ruhr Universität Bochum, Bochum, Germany, 2018.
- [4] S. Askarinejad, V. Deshpande and N. Fleck, *Corros. Sci.*, 2022, **203**, 110356.
- [5] A. Erbe and S. Nayak, in *Encyclopedia of Solid-Liquid Interfaces*, ed. G. Bussetti, K. Wandelt, M.-P. Gaigeot, G. Andersson, H. Bluhm, M. Mezger and D. Starr, Elsevier, Oxford, UK, 2023, ch. Understanding water on surfaces, electrodes, and in bulk by vibrational spectroscopies, pp. in press, DOI: 10.1016/B978-0-323-85669-0.00035-0.
- [6] B. A. Gawel, A. Ulvensøen, K. Łukaszuk, B. Arstad, A. M. F. Muggerud and A. Erbe, *RSC Adv.*, 2020, **10**, 29018–29030.
- [7] J. Creus, A. Perez, C. Berziou, E. Conforto, F. Xavier, C. Rébéré, S. Cohendoz, S. Touzain, F. Sanchette and A. Billard, *NACE: Int. Corros. Conf. Ser.*, 2012, 1568.
- [8] A. Lekatou, A. Sfikas, A. Karantzalis and D. Sioulas, *Corros. Sci.*, 2012, **63**, 193–209.
- [9] H. D. Ruan, R. L. Frost and J. T. Klopogge, *J. Raman Spectrosc.*, 2001, **32**, 745–750.
- [10] R. L. Frost, J. T. Klopogge, S. C. Russell and J. L. Szetu, *Appl. Spectrosc.*, 1999, **53**, 423–434.
- [11] H. Ruan, R. Frost, J. Klopogge and L. Duong, *Spectrochim. Acta A*, 2002, **58**, 265–272.
- [12] S. S. C. Pushparaj, N. D. Jensen, C. Forano, G. J. Rees, V. Prevot, J. V. Hanna, D. B. Ravnsbæk, M. Bjerring and U. G. Nielsen, *Inorg. Chem.*, 2016, **55**, 9306–9315.
- [13] L. Xia and R. L. McCreery, *J. Electrochem. Soc.*, 1998, **145**, 3083–3089.
- [14] M.-C. Jodin-Caumon, B. Humbert, N. Phambu and F. Gaboriaud, *Spectrochim. Acta A*, 2009, **72**, 959–964.
- [15] P. Thomas, V. Ramakrishnan and V. Vaidyan, *Thin Solid Films*, 1989, **170**, 35–40.
- [16] A. Kreta, M. Rodošek, L. Slemenik Perše, B. Orel, M. Gabersček and A. Šurca Vuk, *Corros. Sci.*, 2016, **104**, 290–309.
- [17] A. Kiss, G. Keresztury and L. Farkas, *Spectrochim. Acta A*, 1980, **36**, 653–658.
- [18] T. Schram, J. D. Laet and H. Terry, *J. Electrochem. Soc.*, 1998, **145**, 2733–2739.
- [19] N. J. Cherepy, T. H. Shen, A. P. Esposito and T. M. Tillotson, *J. Colloid Interface Sci.*, 2005, **282**, 80–86.
- [20] P. Tarte, *Spectrochim. Acta A*, 1967, **23**, 2127–2143.

- [21] J. Y. Ying, J. B. Benziger and H. Gleiter, *Phys. Rev. B*, 1993, **48**, 1830–1836.
- [22] C. Dyer, P. J. Hendra, W. Forsling and M. Ranheimer, *Spectrochim. Acta A*, 1993, **49**, 691–705.
- [23] A. S. Barker, *Phys. Rev.*, 1963, **132**, 1474–1481.
- [24] P. Brüesch, R. Kötz, H. Neff and L. Pietronero, *Phys. Rev. B*, 1984, **29**, 4691–4696.
- [25] D. Dohy, G. Lucazeau and D. Bougeard, *Solid State Ionics*, 1983, **11**, 1–18.
- [26] W. W. Rudolph, R. Mason and C. C. Pye, *Phys. Chem. Chem. Phys.*, 2000, **2**, 5030–5040.
- [27] H. Kanno, T. Yamaguchi and H. Ohtaki, *J. Phys. Chem.*, 1989, **93**, 1695–1697.
- [28] G. Melani, Y. Nagata, J. Wirth and P. Saalfrank, *J. Chem. Phys.*, 2018, **149**, 014707.
- [29] Y. Yue, G. Melani, H. Kirsch, A. Paarmann, P. Saalfrank, R. K. Campen and Y. Tong, *J. Phys. Chem. C*, 2022, **126**, 13467–13476.
- [30] L. Vlaev, D. Damyanov and M. Mohamed, *Colloids Surf.*, 1989, **36**, 427–437.
- [31] G. Melani, Y. Nagata and P. Saalfrank, *Phys. Chem. Chem. Phys.*, 2021, **23**, 7714–7723.
- [32] L. Yu, L. Chen, L.-P. Dong, L.-J. Li and Y.-Z. Wang, *RSC Adv.*, 2014, **4**, 17812–17821.
- [33] Y. Yu and Y. Li, *Corros. Sci.*, 2020, **168**, 108568.
- [34] X. Xue and M. Kanzaki, *J. Phys. Chem. B*, 2007, **111**, 13156–13166.
- [35] S. Nayak, P. U. Biedermann, M. Stratmann and A. Erbe, *Phys. Chem. Chem. Phys.*, 2013, **15**, 5771–5781.
- [36] E. Mysliu, K. S. Storli, E. Kjørsvik, O. Lunder and A. Erbe, *J. Electrochem. Soc.*, 2023, **170**, 011503.
- [37] F. R. L. Faulstich, H. V. Castro, L. F. C. de Oliveira and R. Neumann, *Spectrochim. Acta A*, 2011, **80**, 102–105.
- [38] I. Degen and G. Newman, *Spectrochim. Acta A*, 1993, **49**, 859–887.
- [39] J. L. White and S. L. Hem, *J. Pharm. Sci.*, 1975, **64**, 468–469.
- [40] C. J. Serna, J. L. White and S. L. Hem, *Soil Sci. Soc. Am. J.*, 1977, **41**, 1009–1013.
- [41] C. J. Serna, L. J. C., J. L. White and S. L. Hem, *J. Pharm. Sci.*, 1983, **72**, 769–771.
- [42] B. Lafuente, R. T. Downs, H. Yang and N. Stone, in *Highlights in Mineralogical Crystallography*, ed. T. Armbruster and R. M. Danisi, W. De Gruyter, Berlin, Germany, 2015, ch. The power of databases: the RRUFF project, pp. 1–30.
- [43] C. Xu, S. Zhao, Y. Du, W. Zhang, P. Li, H. Jin, Y. Zhang, Z. Wang and J. Zhang, *ChemElectroChem*, 2019, **6**, 3350–3354.

- [44] C. Li, J. Patra, J. Li, P. C. Rath, M.-H. Lin and J.-K. Chang, *Adv. Funct. Mater.*, 2020, **30**, 1909565.
- [45] I. R. Beattie, H. E. Blayden, S. M. Hall, S. N. Jenny and J. S. Ogden, *J. Chem. Soc., Dalton Trans.*, 1976, 666–676.
- [46] H. Edwards, D. Farwell and A. Johnson, *J. Mol. Struct.*, 1995, **344**, 37–44.
- [47] E. Rytter and H. Øye, *J. Inorg. Nucl. Chem.*, 1973, **35**, 4311–4313.
- [48] F. Scholz, W. Unkrig, P. Eiden, M. A. Schmidt, A. Garsuch and I. Krossing, *Eur. J. Inorg. Chem.*, 2015, **2015**, 3128–3138.
- [49] N. Wiberg, *Holleman-Wiberg - Lehrbuch der Anorganischen Chemie, 101st edition*, Walter de Gruyter, Berlin, 1995.
- [50] K. Nakamoto, *Infrared and Raman Spectra of Inorganic and Coordination Compounds*, Wiley, 2008, ch. 2, pp. 275–331.
- [51] R. W. Berg, *Z. Naturforsch. A*, 2007, **62**, 157–168.
- [52] W. W. Lei, D. Liu, P. W. Zhu, X. H. Chen, Q. Zhao, G. H. Wen, Q. L. Cui and G. T. Zou, *Appl. Phys. Lett.*, 2009, **95**, 162501.
- [53] P. Lu, R. Collazo, R. F. Dalmau, G. Durkaya, N. Dietz and Z. Sitar, *Appl. Phys. Lett.*, 2008, **93**, 131922.
- [54] X. Zhang, Z. Liu and S. Hark, *Solid State Commun.*, 2007, **143**, 317–320.
- [55] Q. Wu, Z. Hu, X. Wang, Y. Chen and Y. Lu, *J. Phys. Chem. B*, 2003, **107**, 9726–9729.
- [56] G. G. Perrault, *J. Electrochem. Soc.*, 1979, **126**, 199–204.
- [57] K. R. Hebert, *Electrochim. Acta*, 2015, **168**, 199–205.
- [58] S. Adhikari, J. Ai, K. R. Hebert, K. Ho and C. Wang, *Electrochim. Acta*, 2010, **55**, 5326–5331.
- [59] S. Adhikari, J. Lee and K. R. Hebert, *J. Electrochem. Soc.*, 2008, **155**, C16.
- [60] S. Adhikari and K. R. Hebert, *J. Electrochem. Soc.*, 2008, **155**, C189.
- [61] M. Tkacz, T. Palasyuk, J. Graetz and S. Saxena, *J. Raman Spectrosc.*, 2008, **39**, 922–927.
- [62] A. Giannisi, D. Colognesi, M. Fitchner, E. Röhm, L. Ulivi, C. Ziparo and M. Zoppi, *J. Phys. Chem. A*, 2011, **115**, 691–699.
- [63] C.-p. Wong and P. J. Miller, *J. Energ. Mater.*, 2005, **23**, 169–181.
- [64] T. Kato, Y. Nakamori, S. Orimo, C. Brown and C. Jensen, *J. Alloys Compd.*, 2007, **446-447**, 276–279.
- [65] K. Ikeda, H. Ohshita, N. Kaneko, J. Zhang, M. Yonemura, T. Otomo, K. Suzuya, H. Yukawa, M. Morinaga, H.-W. Li, S. Semboshi and S. ichi Orimo, *Mater. Trans.*, 2011, **52**, 598–601.

- [66] Y. Wang, J.-A. Yan and M. Y. Chou, *Phys. Rev. B*, 2008, **77**, 014101.
- [67] F. S. Manciu, L. Reza, W. G. Durrer, A. Bronson, D. Lacina and J. Graetz, *J. Raman Spectrosc.*, 2011, **42**, 512–516.
- [68] H. Willis, V. Zichy and P. Hendra, *Polymer*, 1969, **10**, 737–746.
- [69] X. Xingsheng, M. Hai, Z. Qijing and Z. Yunsheng, *J. Opt. A*, 2002, **4**, 237–242.